Climate Dynamics
https://doi.org/10.1007/s00382-024-07215-0

ORIGINAL ARTICLE

Projected changes of compound droughts and heatwaves in China under 1.5 °C, 2 °C, and 3 °C of global warming

Taizheng Liu[1] · Yuqing Zhang[2] · Bin Guo[1] · Yu Yin[1] · Jing Ge[3]

Received: 15 December 2023 / Accepted: 24 March 2024

Abstract
Compound drought and heatwave (CDH) events have become increasingly frequent and severe under global warming, with negative impacts on agriculture, ecology, and society. We quantified the changes of CDH events with different magnitudes (severities) across China at global warming thresholds of 1.5 °C, 2 °C, and 3 °C based on 12 Coupled Model Intercomparison Project Phase 6 (CMIP6) model simulations. The results indicated that mild, moderate, severe, and extreme CDH events can increase significantly from 1.5 °C to 3.0 °C of global warming. The frequencies and magnitudes of CDH events during 3 °C warming period are 323.7% and 130.2% higher than those of 1.5 °C warming period. The area impacted by CDH events has expanded, with the increase during 3 °C warming period being nearly threefold that of 1.5 °C warming period. Moreover, the first CDH event will start earlier in a year, while the last event will take place later. This pattern of earlier or later onset is particularly notable with increasing temperatures, especially in northwestern parts of China (NWC). In NWC, the first or last CDH event will occur 2 months earlier or later during 3 °C warming period compared to historical period. The findings highlight the possible implications of global warming at different levels on CDH events in China and the urgency of taking effective measures to mitigate the impacts.

Keywords Compound drought and heatwave · Global warming · CMIP6 · China

1 Introduction

Weather and climate extremes adversely impact ecosystems and society (Su et al. 2018; Luo et al. 2022). Drought is considered one of the most catastrophic climate hazards, severely threatening food, economic, and ecological security (Wang et al. 2022). Similarly, heatwaves can induce water shortages and trigger heat-related illnesses (Matthews et al. 2017; Zampieri et al. 2017). When heatwaves and droughts coincide, termed compound droughts and heatwaves (CDH), the resultant impact typically exceeds that of either phenomenon alone (Zscheischler et al. 2018; Zhang et al. 2022a). This exacerbation is due to the negative correlation between precipitation and temperature, leading to a mutual intensification of both droughts and heatwaves (Adler et al. 2008; Kong et al. 2020). Recently, CDH events have garnered increased attention due to their devastating consequences (Mukherjee et al. 2020; Wang et al. 2021; Zhang et al. 2022a). To enhance our comprehension of CDH events, it is crucial to project the potential changes in CDH events in the future.

Human activities contribute to global warming via greenhouse gas emissions (Sun et al. 2016; Byrne and O'Gorman 2018), leading to significant escalations in climate-related disasters with profound repercussions for both nature and human livelihoods (Su et al. 2018; Zhang et al. 2022c). In response to the detrimental impacts of global warming, the international community has set targets to limit temperature increases to 1.5 °C and 2 °C (UNFCCC 2015). The global average temperature increased by approximately 1 °C during 2001–2020 compared to pre-industrial levels (IPCC 2021), with projections indicating a rise of more than 3 °C by 2100 in high-emission climate scenarios (Zhang et al. 2022c). Each 0.5 °C increase in global temperature represents

✉ Bin Guo
guobin07@mails.ucas.ac.cn

[1] College of Geodesy and Geomatics, Shandong University of Science and Technology, Qingdao 266590, China

[2] School of Geography and Planning, Huaiyin Normal University, Huai'an 223300, China

[3] School of Agriculture, Ningxia University, Yinchuan 750021, China

Published online: 10 April 2024

substantial changes in the energy dynamics of the climate system (Hare et al. 2016). As global warming approaches 2–3 °C, numerous ecologically vulnerable nations worldwide will face heightened risks of severe climate-related disasters. Yang et al. (2018) demonstrated that a 2 °C rise in global temperatures could increase the frequency and severity of temperature extremes in China by 32–34% relative to a 1.5 °C increase. King et al. (2017) suggested that limiting warming to 1.5 °C could significantly reduce the occurrence of extreme events. Thus, keeping average temperature increases within 1.5 °C rather than 2 °C could significantly lessen the impact of climate change (Hare et al. 2016; Schleussner et al. 2016). China is experiencing faster warming compared to the global average, facing heightened risks of warming-induced disasters (Zhang et al. 2019). Recent years have seen a rise in the frequency of heatwaves across China, affecting large areas (Sun et al. 2014). The 2022 summer heatwave in eastern China (EC) exemplifies this trend, exposing over 270 million people to extreme heat (Yin et al. 2023). Moreover, warmer temperatures leading to increased evapotranspiration exacerbate drought intensity (Nam et al. 2015). The interaction between high temperatures and precipitation deficits can precipitate CDH events. Therefore, it is imperative to analyze the variations in CDH events in China under global warming scenarios of 1.5 °C, 2 °C, and 3 °C.

The frequency of CDH events has increased due to global warming (IPCC 2021). Min et al. (2023) observed a pervasive uptrend in the likelihood of CDH occurrences globally from 1902 to 2019. Wu et al. (2021) examined CDH events across terrestrial areas worldwide between 1950 and 2019, finding that numerous regions, particularly in China, the United States, and Australia, have experienced increasingly severe CDH events. In recent years, there has been a growing number of studies focusing on changes in CDH events in China due to their more serious threat to socio-economic stability and human security (Chen and Sun 2017; Chen et al. 2019; Li et al. 2019). For example, Kong et al. (2020) assessed changes in CDH events in EC during 1962–2015. Li et al. (2019) identified an upward trend in CDH events in Northwest China between 1961 and 2017. Wu et al. (2019b) reported a significant increase in the frequency of CDH events in China during 1988–2014 compared to 1961–1987. However, previous studies have primarily focused on assessing changes in the frequency and magnitude of CDH events in historical periods, without sufficient attention given to future changes, especially under different warming levels. Moreover, understanding of shifts in CDH onset dates under different future warming scenarios remains limited.

The Coupled Model Intercomparison Project Phase 6 (CMIP6) serves as a crucial tool for evaluating climate change. In contrast to CMIP5, CMIP6 incorporates more intricate physical processes and offers much higher resolution (Forster et al. 2020). As a result, CMIP6 is more effective in providing valuable information when simulating climate extremes. It integrates shared socioeconomic pathways (SSPs) with representative concentration pathways (RCPs) to develop more comprehensive climate prediction scenarios (Meinshausen et al. 2020). These scenarios delineate varying emission targets that are expected to be achieved. Commonly-used future scenarios include SSP1-2.6, SSP2-4.5, and SSP5-8.5. Scenario SSP1-2.6 combines SSP1 and RCP2.6, representing a low-emission pathway. SSP2-4.5 represents a medium pathway aligned with current societal development trends. SSP5-8.5 signifies a high-emission route characterized by extensive fossil fuel combustion (Zhuang et al. 2021). Our focus is on examining changes in CDH events at distinct warming levels of 1.5 °C, 2 °C, and 3 °C based on various future emission scenarios.

This study utilized 12 CMIP6 models to predict changes in CDH events of varying severities at warming targets of 1.5 °C, 2 °C, and 3 °C. The primary goals of this study are as follows: (1) assessing CMIP6 performance in simulating temperature and precipitation; (2) identifying the years when the global mean temperature exceeds the thresholds of 1.5 °C, 2 °C, and 3 °C above pre-industrial levels under diverse future scenarios; (3) projecting CDH events with different magnitudes under 1.5 °C, 2 °C, and 3 °C warming targets.

2 Materials and methods

2.1 Gridded-observed data

The daily CN05.1 dataset (0.25°), which is constructed with approximately 2400 stations, is provided by the Climate Change Research Center, Chinese Academy of Sciences (Wu and Gao 2013). This dataset has been extensively utilized for the exploration of extreme events in China (Yang et al. 2018; Su et al. 2022). This study utilizes CN05.1 data, including precipitation, mean temperature (T_{ave}), and maximum temperature (T_{max}) from 1961 to 2014, as observational data. To match the resolution of the model data, the CN05.1 dataset is upscaled to a 0.5° × 0.5° grid using the bilinear interpolation method.

2.2 CMIP6 model simulations

Daily precipitation, T_{ave}, and T_{max} are obtained from 12 CMIP6 model simulations (https://esgf-node.llnl.gov/search/cmip6/). These simulations include both historical

scenarios (1850–2014) and future scenarios (SSP1-2.6, SSP2-4.5, and SSP5-8.5 during 2015–2099). Considering the resolution disparities among the model simulations, a bilinear interpolation method is employed to interpolate the data to a resolution of 0.5° (Zhang et al. 2023). Additional details regarding these models are shown in Table 1.

Table 1 CMIP6 models used in this study

Model	Institute	Resolution (lon×lat)	Realization
BCC-CSM2-MR	Beijing Climate Center (BCC), China	320×160	r1i1p1f1
CAMS-CSM1-0	Chinese Academy of Meteorological Sciences, China	320×160	r2i1p1f1
CMCC-ESM2	Fondazione Centro Euro-Mediterraneo Sui Cambiamenti Climatici (CMCC), Italy	288×192	r1i1p1f1
CNRM-CM6-1	Centre National de Recherches Meteorologiques (CNRM) and Centre European de Recherche et de Formation Avance en Calcul Scientifique (CERFACS), France	256×128	r1i1p1f2
EC-Earth3	EC-Earth-Consortium, Europe	512×256	r1i1p1f1
EC-Earth3-Veg-LR		320×160	r1i1p1f1
GFDL-ESM4	Geophysical Fluid Dynamics Laboratory (NOAAGFDL), USA	288×180	r1i1p1f1
MIROC6	National Institute for Environmental Studies (NIES) and RIKEN Center for Computational Science (RCCS), Japan	256×128	r1i1p1f1
MPI-ESM-1-2-HR	Max Planck Institute for Meteorology (MPI-M), Germany	384×192	r1i1p1f1
MRI-ESM2-0	Meteorological Research Institute (MRI), Japan	320×160	r1i1p1f1
NorESM2-MM	Norwegian Climate Centre, Norway	288×192	r1i1p1f1
TaiESM1	Research Center for Environmental Changes, Academia Sinica, Taipei, China	288×192	r1i1p1f1

2.3 Global warming levels

We employed the T_{ave} 30-year running mean method to determine global warming thresholds under various future scenarios (Vautard et al. 2014; Zhang et al. 2019). The 1.5 °C warming period refers to the period during which the T_{ave} increases by 1.3–1.7 °C relative to the pre-industrial benchmark (1850–1900) (King et al. 2017; Zhang et al. 2019). Similarly, thresholds for the 2 °C and 3 °C periods are established, corresponding to T_{ave} increments of 1.8–2.2 °C and 2.8–3.2 °C, respectively. The period 1981–2010 serves as the historical reference period for this study.

2.4 CDH definition

Monthly T_{ave} and precipitation data are extracted from the outputs of 12 daily CMIP6 models to calculate the 1-month Standardized Precipitation Evapotranspiration Index (SPEI), thereby facilitating the identification of drought events. A threshold of -0.8 (SPEI < -0.8) is adopted to determine the occurrence of droughts (Wang et al. 2021), indicating that an SPEI value below -0.8 represents a drought event. Similarly, heatwaves are defined as periods during which daily T_{max} exceeds a specific threshold for three or more consecutive days (Mukherjee et al. 2020; Zhang et al. 2022b). The 95th percentile of T_{max} during the warm season (May–October) for the reference period (1981–2010) serves as the temperature threshold for each grid (Yu and Zhai 2020; Wang et al. 2021). Subsequently, a CDH event is identified when a heatwave occurs within a dry month characterized by an SPEI < -0.8 (Wang et al. 2021). If a heatwave extends across two different months, it is assigned to the month in which it starts. This study specifically focuses on CDH events that occur from May to October each year. We utilized relative change rates to assess variations in CDH events across distinct warming periods. The changes in CDH events during 1.5 °C (2 °C and 3 °C) period represent the average change across three scenarios (SSP1-2.6, SSP2-4.5, and SSP5-8.5) for this specific period. The frequency of CDH events is defined as the total number of such events within a year.

The drought severity ($|\Delta D|$) is quantified by the difference between the drought indicator (D_r) and the drought threshold (D_{th}, -0.8), where larger differences indicate more severe drought conditions (Wu et al. 2019a). Similarly, the magnitude of a hot day (ΔT) is assessed by the bias of T_{max} from the temperature threshold (T_{95th}) during a heatwave, with the cumulative magnitude of hot days representing the overall magnitude of the heatwave. As these two metrics are measured in different units, normalization is applied to convert the magnitude of droughts and heatwaves into $P_D(|\Delta D|)$ and $P_T(\Delta T)$, respectively (Zhang et al. 2021). To

avoid misclassifying mild droughts as non-drought events due to a normalized result of 0, this study adopts a normalization range of [0.1,1]. Thus, the Compound Drought and Heatwave Magnitude Index (CDHMI) is defined using the following formula (Fig. 1):

$$\begin{aligned} \mathrm{CDHMI} &= P_D\left(|D_r - D_{th}|\right) P_T \left[\sum_{i=1}^{n}\left(T_{\max(i)} - T_{95th}\right)\right] \\ &= P_D\left(|\Delta D|\right) P_T \left[\sum_{i=1}^{n} \Delta T_i\right] \end{aligned} \quad (1)$$

where i is day i within the heatwave period and n is the total number of hot days.

3 Results

3.1 Evaluation of CMIP6 in simulating precipitation and temperature

To evaluate the performance of CMIP6 models in simulating meteorological variables, we made the comparisons of multi-year mean precipitation, T_{ave}, and T_{max} for the reference period (1981–2010) between CN05.1 and CMIP6 model simulations. The multi-model ensemble average (MME) of precipitation adequately captures the spatial distribution of observed data (Fig. 2a–b), showing high values (> 1400 mm) in southeastern parts of China and low values (< 300 mm) in northwestern parts of China (NWC). Most CMIP6 climate models accurately simulate precipitation characteristics in NWC and northern parts of China (NC), with bias ranging from − 100 to 100 mm (Fig. S1, Supporting Information). The spatial pattern of MME T_{ave} generally aligns with observational data, exhibiting a decrease with increasing latitude (Fig. 2c–d). However, CMIP6 models tend to underestimate T_{ave} in the Tibetan Plateau, while showing minor bias (− 1 °C to 1 °C) in EC (Fig. S2, Supporting Information). Similar to T_{ave}, the spatial pattern of T_{max} is effectively captured by MME results (Fig. 2e–f), with most CMIP6 models displaying consistent simulations except for MIROC6, which tends to overestimate T_{max} (Fig. S3, Supporting Information). The comparison in Fig. S4 reveals that the models generally overestimate observed precipitation by less than 30%, apart from CMCC-ESM2, MIROC6, and TaiESM1. While both T_{ave} and T_{max} simulated by the MME are approximately 1 °C and 2 °C lower than the observed values, respectively. Overall, MME results of CMIP6 can well reflect precipitation and temperature characteristics and are reliable for future projections.

3.2 Time periods for 1.5 °C, 2.0 °C, and 3.0 °C of global warming

The global T_{ave} anomaly remains relatively stable in the latter half of the 21st century under SSP1-2.6 scenario, exhibiting an increase of approximately 2.3 °C compared to the period of 1850–1900 (Fig. 3). This sustainable development pathway remains well below the critical 3 °C warming

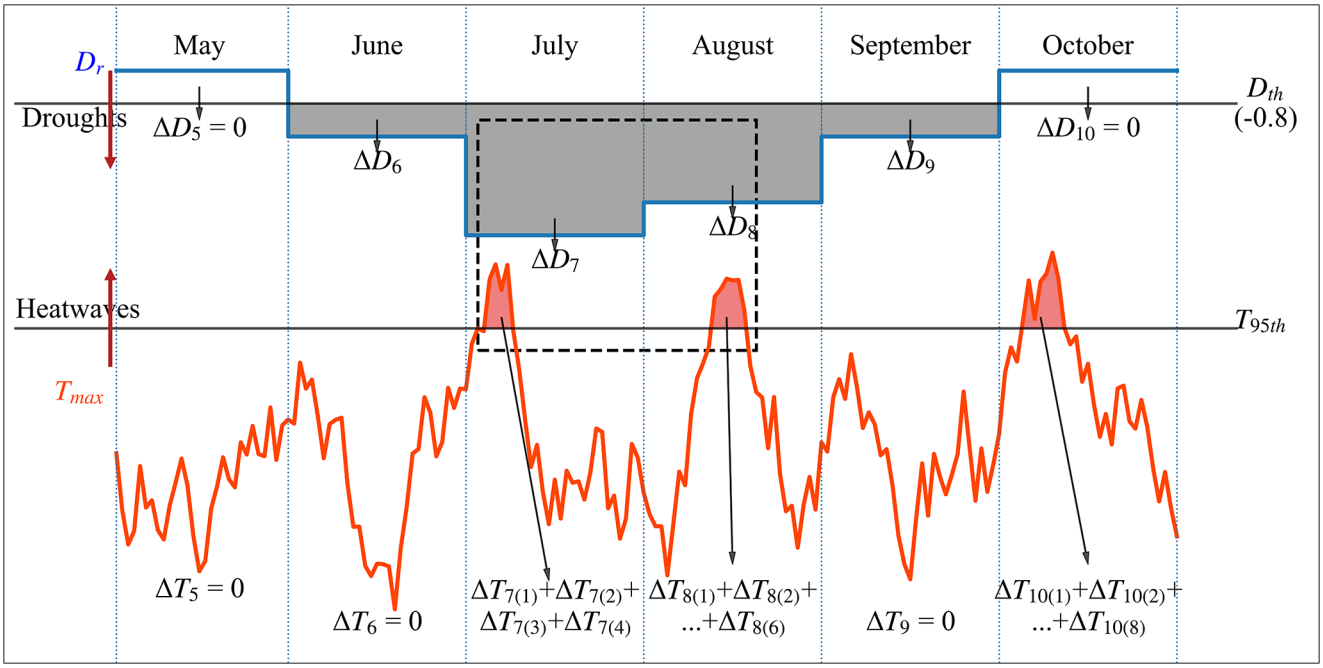

Fig. 1 Schematic diagram of CDHMI based on SPEI and T_{max}

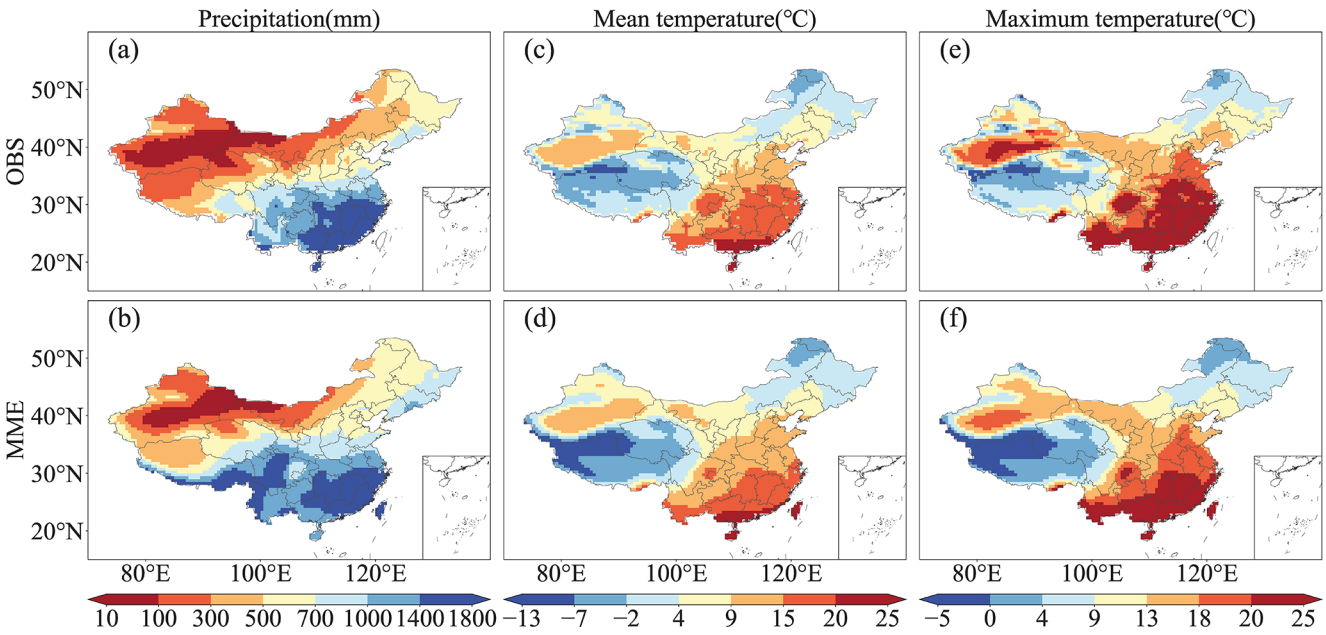

Fig. 2 Spatial patterns of 30-year mean (a–b) precipitation, (c–d) T_{ave}, and (e–f) T_{max} in China during 1981–2010 from observation (CN05.1) and MME of CMIP6, respectively

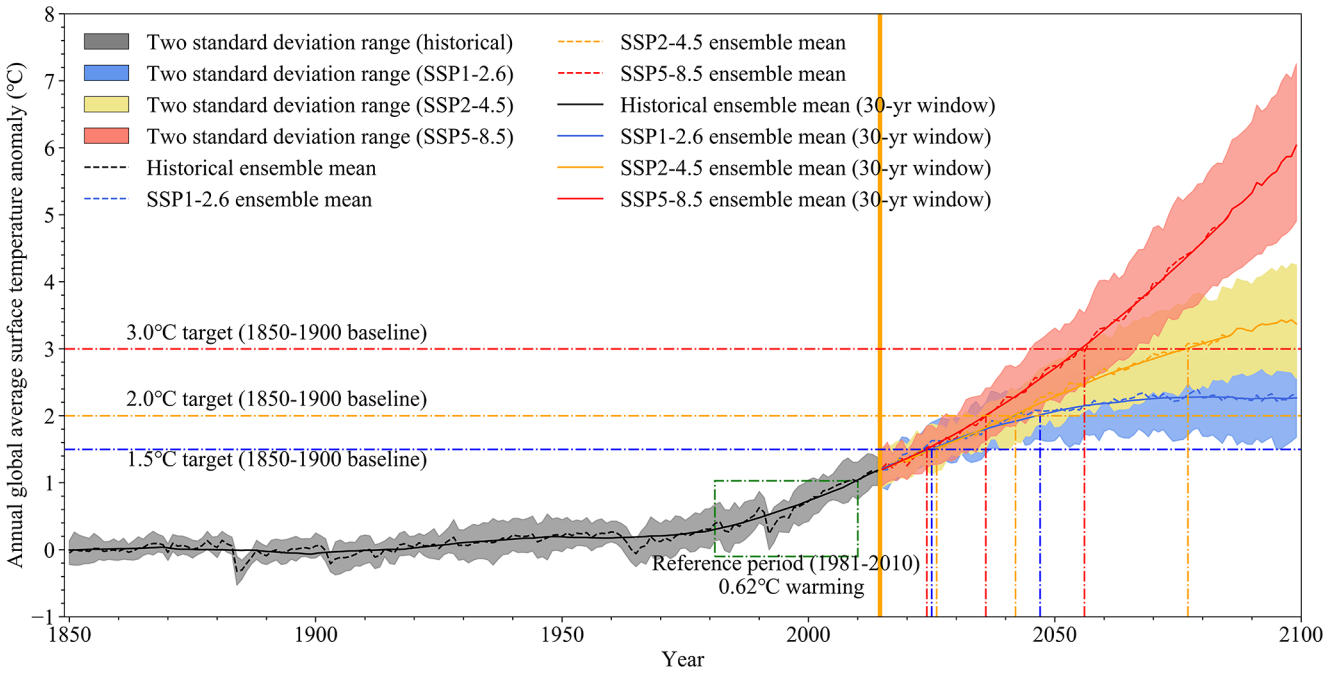

Fig. 3 Annual global mean temperature anomaly based on MME simulation. The bold yellow vertical line is the boundary between the historical and future periods

threshold. In contrast, temperature increases under SSP5-8.5 and SSP2-4.5 scenarios outstrip those of SSP1-2.6, reaching around 6 °C and 3.3 °C, respectively, by the end of 21st century. These projections far exceed our expected warming targets. Temperatures have risen by about 0.6 °C in the reference period (1981–2010) compared to the period of 1850–1900.

Specific warming thresholds are reached earlier under SSP5-8.5 compared to SSP1-2.6 and SSP2-4.5 (Table S1 and Fig. 3). SSP1-2.6 scenario is projected to reach 1.5 °C (1.3–1.7 °C) target in 2025 (2018–2032), very close to 2026 (2019–2033) for SSP2-4.5 and 2024 (2019–2030) for SSP5-8.5. The 2 °C (1.8–2.2 °C) target under SSP1-2.6 is achieved in 2047 (2036–2063), which is 5 years later than 2042

(2036–2048) projected under SSP2-4.5 and 11 years later than 2036 (2032–2041) under SSP5-8.5. Both SSP2-4.5 and SSP5-8.5 are projected to encounter the 3 °C (2.8–3.2 °C) threshold in 2077 (2068–2086) and 2056 (2052–2059), respectively, with a 21-year discrepancy in reaching this level.

3.3 Changes in CDH events under global warming levels of 1.5 °C, 2 °C, and 3 °C

The frequency of CDH events exhibits significant upward trends under three future scenarios, with the rate of increase correlating with the magnificent of warming (Fig. 4a). Under SSP5-8.5 scenario, the growth in CDH frequency is most pronounced (0.216 events/decade), surpassing the increases under SSP2-4.5 (0.109 events/decade) and SSP1-2.6 (0.035 events/decade). Notably, the increases in CDH frequency under SSP1-2.6 stabilize after the 2060s. By 2100, the annual frequency of CDH events under SSP1-2.6 is expected to increase by approximately 0.5 events compared to the reference period. In contrast, the frequency of CDH events will increase by approximately 1.8 events under SSP5-8.5 compared to the reference period. As shown in Fig. 4b, consistent with CDH frequency, the magnitudes across all three future scenarios exhibit significant ($P < 0.05$) upward trends. Among these scenarios, SSP5-8.5 exhibits the most pronounced increase. Specifically, annual magnitudes of CDH events are projected to increase at rates of 0.009/decade under SSP1-2.6, 0.024/decade under SSP2-4.5, and 0.040/decade under SSP5-8.5.

We investigated the changes in both the frequency and magnitude of CDH events at warming thresholds of 1.5 °C, 2 °C, and 3 °C relative to reference period. These changes were calculated by subtracting reference period values from those during the warming period and subsequently dividing by the reference period values. During the reference period, the frequency of CDH events was notably high in EC, with most of EC experiencing a frequency greater than 0.30 events/year (Fig. S5, Supporting Information). Conversely, the frequency was relatively low in NWC. The regions with relatively high magnitude were predominantly located in NC, while CDH events in NWC and central China were less

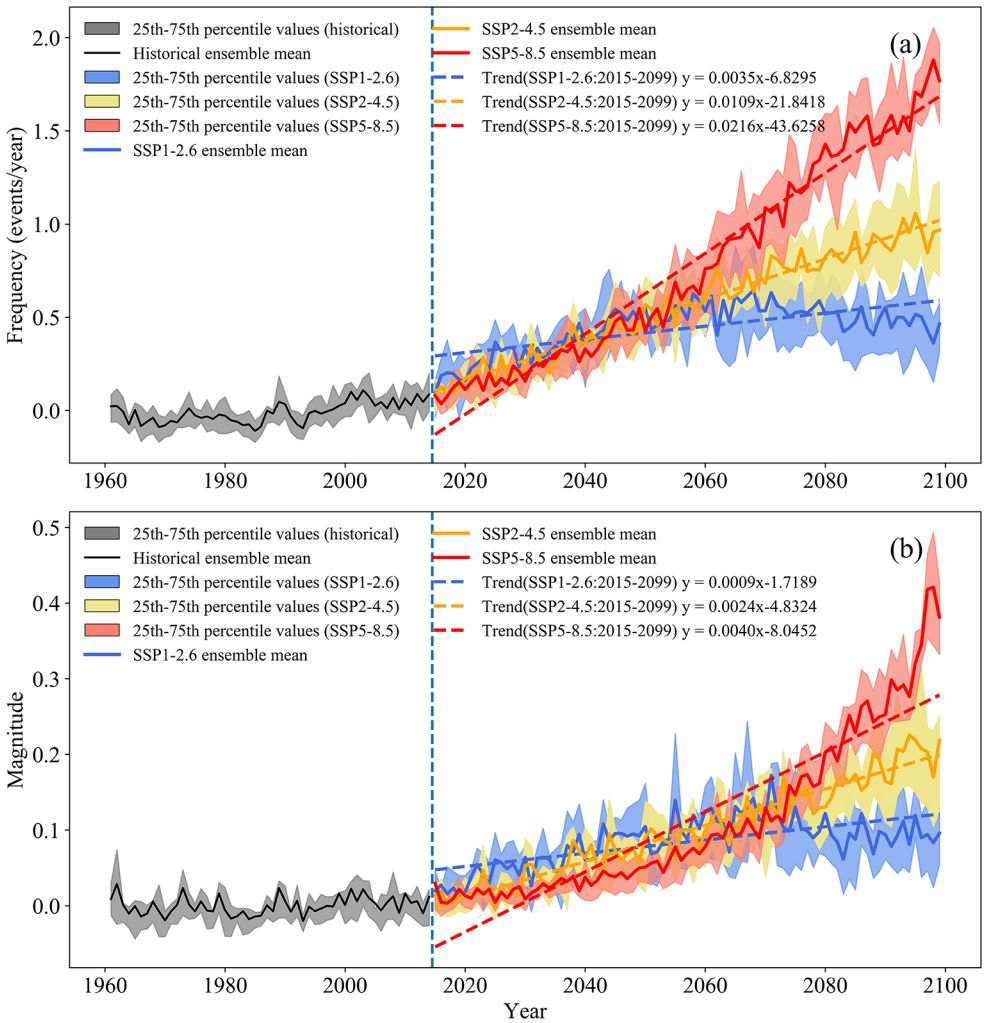

Fig. 4 Annual (a) frequency and (b) magnitude anomalies of CDH events during 1961–2099 (reference period: 1981–2010). The linear trend passed the 0.05 significance test.

intense. Overall, as temperatures rise, the frequency of CDH events is expected to increase steadily. The large increases in frequency of CDH events are observed in NWC, with increments of over 400% during warming periods of 2 °C and 3 °C (Fig. 5a–c). Even during the 1.5 °C period, most regions in NWC experience increases of over 150%. Frequency increases in southern parts of China (SC) are slightly smaller than those in NWC. During 1.5 °C period, frequency increments in most parts of SC range from 0 to 200%, increasing to 150–250% during 2 °C period, and exceeding 250% during 3 °C period. The spatial mean frequency increments during the 3 °C period (468.4%) far exceed those during the 2 °C (267%) and 1.5 °C (144.7%) periods. Frequency simulations from most CMIP6 models exhibit similar spatial increase characteristics to MME, with relatively high increases concentrated in NWC (Figs. S6–S8, Supporting Information). The magnitude increments of CDH events are slightly lower than the frequency increments for the same period (Fig. 5d–f). Similarly, NWC is also a region of high increases in the magnitude of CDH events. The spatial mean magnitude increment during the 1.5 °C period is 55.3%, rising to 107.3% and 185.5% during the 2 °C and 3 °C periods, respectively. These findings underscore the substantial impact of warming on CDH events.

To explore changes in the timing of CDH events under different warming levels, we calculated the differences in occurrence months of the first and last CDH events between future warming periods and historical periods. During the 1.5 °C period, approximately 13.86% of the grids experience an earlier occurrence of the first CDH event, especially in NWC (Fig. 6a). As warming increases to 2 °C, the proportion of grids exhibiting an earlier first CDH event rises to 40.63% compared to 1981–2010, with the first CDH event occurring 2 months earlier than the historical period at approximately 1.90% of the grids (Fig. 6b). This indicates an expansion of the region experiencing earlier first CDH events during the 2 °C period compared to the 1.5 °C period. Upon reaching a warming of 3 °C, the majority of regions (71.61%) experience an earlier occurrence of the first CDH event relative to the historical period (Fig. 6c). The number of regions experiencing a 2-month difference in the onset month of the first CDH event between the 3 °C period and historical period is relatively high (7.24%). Conversely, in a warming climate, the occurrence of the last CDH event each year is delayed compared to historical period, with this delay more pronounced at higher levels of warming. Specifically, during 1.5 °C period, approximately 26.13% of grid areas exhibit a later occurrence of the last CDH event compared to 1981–2010 (Fig. 6d). This proportion increases to 64.03% at 2 °C warming (Fig. 6e). The tendency for the last CDH event to occur later intensifies further during the 3 °C period (Fig. 6f). CMIP6 model simulations also indicate that under global warming, the months in which the first and last CDH events occur are expected to shift earlier and later, respectively (Figs. S9–S14, Supporting Information). These findings highlight the significant impact of warming on the timing of CDH events, with earlier occurrences of the first event and delayed occurrences of the last event observed as warming levels increase.

The percentage changes in the area affected by CDH events are defined similarly to frequency changes. Given that SSP1-2.6 scenario fails to surpass the 3 °C threshold by 2100, changes in area affected by CDH events during the 3 °C warming period are only considered for SSP2-4.5 and SSP5-8.5 scenarios. As warming increases from 1.5 °C to 3 °C, a growing number of regions will face CDH events (Fig. 7). The expansion of areas impacted by CDH events across the three future scenarios remains relatively consistent

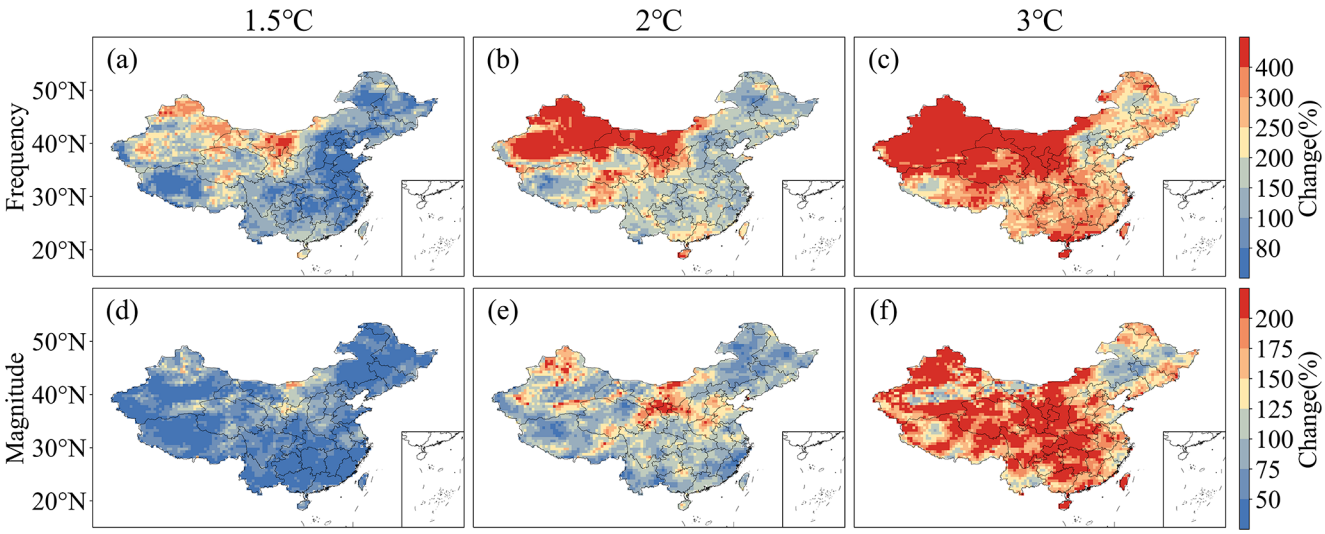

Fig. 5 Changes (%) in CDH (a–c) frequency and (d–f) magnitude at 1.5 °C, 2 °C, and 3 °C targets compared to 1981–2010

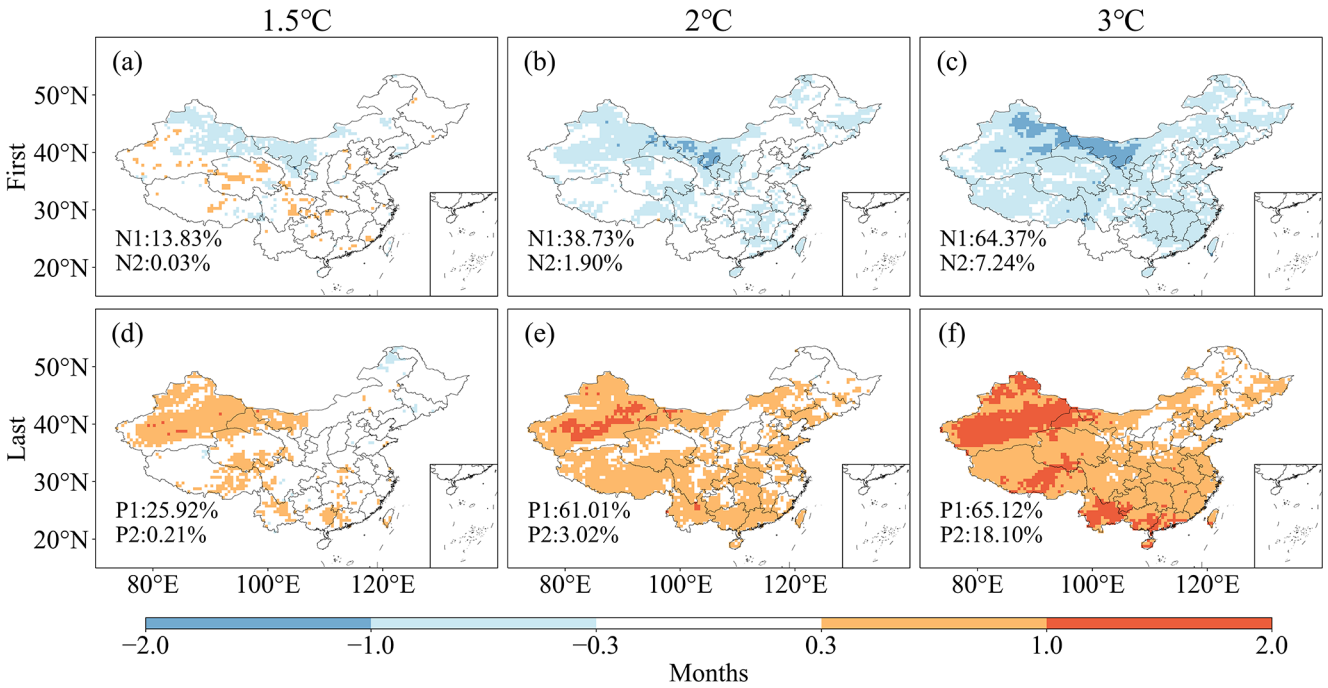

Fig. 6 Difference of occurrence month of (a–c) first and (d–f) last CDH events under warming targets of 1.5 °C, 2 °C, and 3 °C compared to reference period (1981–2010). N denotes a negative value indicating an earlier occurrence of CDH events. N1 and N2 denote the percentage of grids with differences falling within the ranges of [−1, −0.3) and [−2, −1), respectively, relative to the total number of grids. P denotes a positive value indicating a later occurrence of CDH events. P1 and P2 denote the percentage of grids with differences falling within the ranges of (0.3, 1] and (1, 2], respectively, relative to the total number of grids

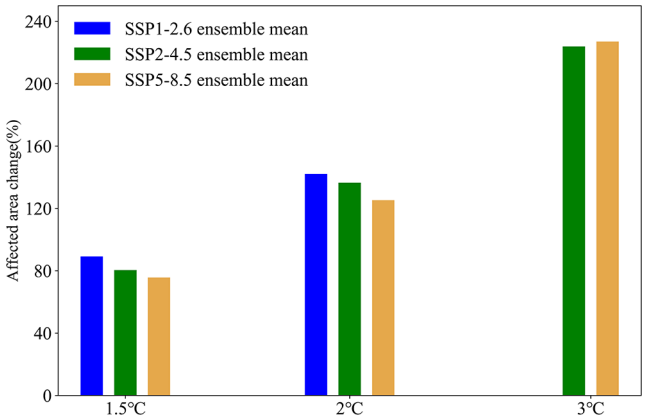

Fig. 7 Changes in area affected by CDH events for different future scenarios under warming targets of 1.5 °C, 2 °C, and 3 °C compared to 1981–2010. The SSP1-2.6 scenario does not meet 3 °C threshold by 2100

during the 1.5 °C period, approximately 80%. During the 2 °C period, the affected area has expanded by 142% under SSP1-2.6, 136% under SSP2-4.5, and 125% under SSP5-8.5 compared to the reference period (1981–2010). Once warming reaches 3 °C, the affected area in SSP2-4.5 and SSP5-8.5 scenarios increases by approximately 220% compared to 1981–2010, and the increments of affected area in these two scenarios are about 3 times that of 1.5 °C period. Each CMIP6 model also exhibits substantial increases in the area affected by CDH events with warming levels (Fig. S15, Supporting Information). The CMCC-ESM2 model exhibits the least change in the affected area during the 1.5 °C period, with a merely 37.56% increase. The affected area of this model expands by 134.87% during the 2 °C period compared to 1981–2010. During the 3 °C period, the increases in the affected area (215.91%) reach approximately sixfold that of the 1.5 °C period.

3.4 Characteristics of CDH events with different magnitudes

The CDHMI values are categorized into 4 classes based on probability density of CDHMI values associated with CDH events that occurred across all grids during the reference period. These three classification thresholds, i.e., 0.05, 0.09, and 0.18 correspond to probability densities of 0.51, 0.78, and 0.93, respectively, which represent nearly half, the majority, and nearly all CDH event cases, respectively. We categorize events with CDHMI values ranging from 0.01 to 0.05 as mild events, from 0.05 to 0.09 as moderate events, from 0.09 to 0.18 as severe events, and those exceeding 0.18 as extreme events.

As shown in Fig. 8, the increases in mild CDH events are particularly evidence in NWC. The spatially mean increments in frequency of mild CDH events during the 1.5 °C

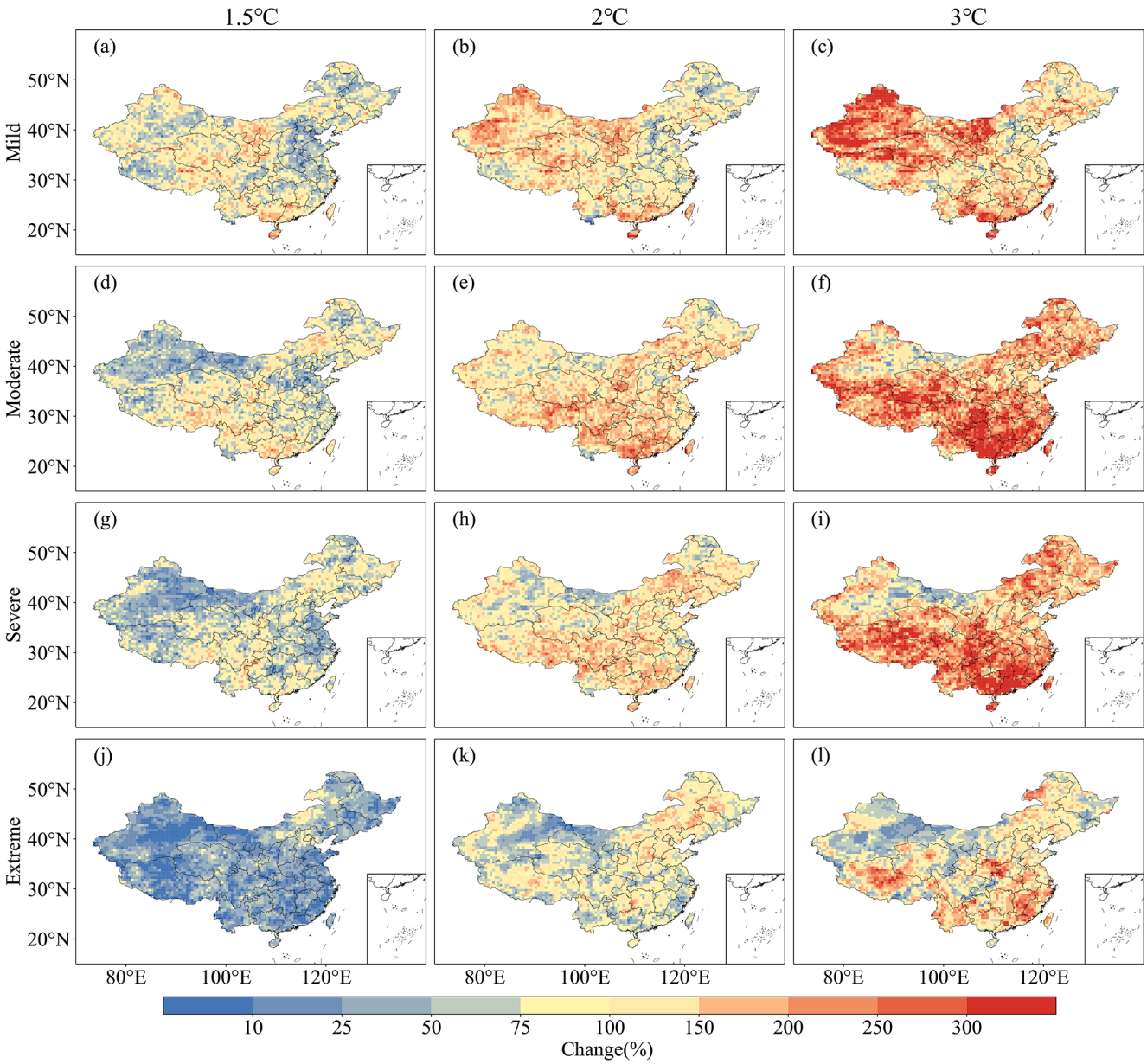

Fig. 8 Frequency change (%) of (a–c) mild, (d–f) moderate, (g–i) severe, and (j–l) extreme CDH events under the three warming targets compared to 1981–2010

period compared to 1981–2010 is 91.8%. The mean increment during the 2 °C period (127.1%) is slightly larger than that during the 1.5 °C period. During the 3 °C period, the mean increments in frequency of mild events (180%) are nearly twice that during the 1.5 °C period. The spatial pattern of frequency increments for moderate CDH events differs from that of mild events, with large values concentrated in SC. The frequency increments of moderate CDH events in NWC are relatively small. For example, during the 1.5 °C period, the frequency increments of moderate events in NWC remain below 75%, whereas those in SC surpass 100%. The average frequency increments of moderate events gradually increase, reaching 84.3% during the 1.5 °C period, 135.8% during the 2 °C period, and 207.9% during the 3 °C period. The average increment of moderate events during the 3 °C period surpasses that of mild events. The spatial patterns of frequency increases for severe CDH events are similar to those of moderate events, with large increments observed in SC. The mean frequency increments of severe events during the three warming periods are 66.8%, 121.4%, and 195.4%, respectively. Moderate and severe events exhibit a more rapid increase compared to mild events, with mean frequency increments during the 3 °C period approaching triple that of the 1.5 °C period. The increases in frequency

of extreme CDH events are slightly smaller than that of other three grades of CDH events. During the 1.5 °C period, the spatial average increase in extreme CDH frequency is relatively low, at just 30% compared to 1981–2010. As the warming progresses to 2 °C and 3 °C periods, the frequency increments of extreme CDH events increase to 85.4% and 113.8%, respectively.

The spatial areas affected by CDH events with the four magnitudes consistently exhibit upward trends as warming increases from 1.5 °C to 3 °C (Fig. 9). Specifically, the areas affected by mild CDH events increase by 59%, 86%, and 133% under warming levels of 1.5 °C, 2 °C, and 3 °C, respectively. The increments in area affected by moderate CDH events during the 3 °C period (317%) are nearly twice that during the 2 °C period (168%) and approximately three times that during the 1.5 °C period (96%), respectively. The spatial areas affected by extreme CDH events exhibit the highest increments compared to other magnitudes of CDH events, reaching 165% at 1.5 °C, 390% at 2 °C, and a remarkable 997% at 3 °C. This may be attributed to the fact that extreme CDH events occurred less frequently than mild and moderate CDH events during the historical period, leading to a more pronounced increase in affected areas as warming intensifies.

Finally, we investigated the temporal changes in the first and last CDH events with four magnitudes. Rising temperatures lead to an earlier occurrence of the first CDH events per year (Fig. 10). During the 1.5 °C period, approximately 7.19% of the grids demonstrate an earlier first mild event compared to the historical period, primarily concentrated in NWC (Fig. 10a). Conversely, around 18.96% of the grids exhibit a later first mild event. As warming increases to the 2 °C level, the proportion of grids experiencing earlier first mild events rises to 24.17%, while those experiencing later first mild events decrease to 4.98% (Fig. 10b). This indicates an expanding region of earlier first mild events, especially in

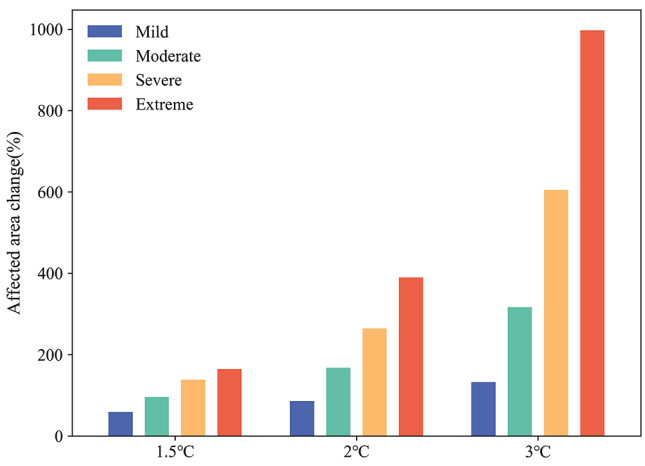

Fig. 9 Changes (%) in the area affected by CDH events with the four magnitudes under the three warming targets compared to 1981–2010

NWC. A further expansion of areas experiencing earlier first mild events is observed during the 3 °C period (Fig. 10c). During this warming period, about 33.79% of grids experience earlier first mild events (<-0.3), with about 2.92% of the grids exhibiting onset month differences of less than -1. This indicates that the advancement of the first mild event is more pronounced during higher warming periods. The spatial patterns of onset month differences for the first moderate CDH events follow a similar trend to those of first mild CDH events. Early onset of the first moderate event per year is first observed in NWC, with the proportion of grids experiencing earlier first moderate events reaching 14.02%, 40.48%, and 54.86% across the three warming periods, respectively (Fig. 10d–f). The proportion of grids where the first moderate event occurs two months earlier than the historical period (occurrence month difference <-1) increases to 0.16%, 2.40%, and 4.90%, respectively. This further underscores the increasing magnitude of advancement. Similarly, the first severe and extreme events exhibit comparable advanced characteristics to the mild events (Fig. 10g–l).

Figure 11 shows the difference in occurrence month of the last CDH event with different magnitudes under the three warming targets compared to 1981–2010. As temperatures rise, there is a clear tendency for the last CDH events to occur in later months of the year. Approximately 19.72% of regions experience a delayed occurrence of the last mild event during the 1.5 °C warming period compared to the historical period, while approximately 8.73% of regions record an earlier occurrence. This implies a heightened likelihood of the last mild event happening in subsequent months of the year due to global warming. As warming escalates to 2 °C (3 °C), approximately 47% (62.52%) of regions exhibit a later occurrence of the last mild event. Among these regions, the proportion experiencing a two-month delay compared to the historical period stands at 4.85% and 15.11%, respectively. These regions with significant monthly differences (>1) are primarily concentrated in NWC. The last moderate, severe, and extreme events exhibit similar delayed onset trends as the last mild event, with more pronounced delays in NWC and SC. Across the three warming periods, regions experiencing a later onset of the last extreme event account for 29.04%, 65.54%, and 72.25% of China, respectively. Among these regions, those experiencing onset month differences exceeding one month comprise 1.90%, 8.78%, and 20.60%, respectively.

4 Discussion

The global climate system is experiencing unprecedented transformations, profoundly impacting both natural ecosystems and human societies. Notably, there has been a

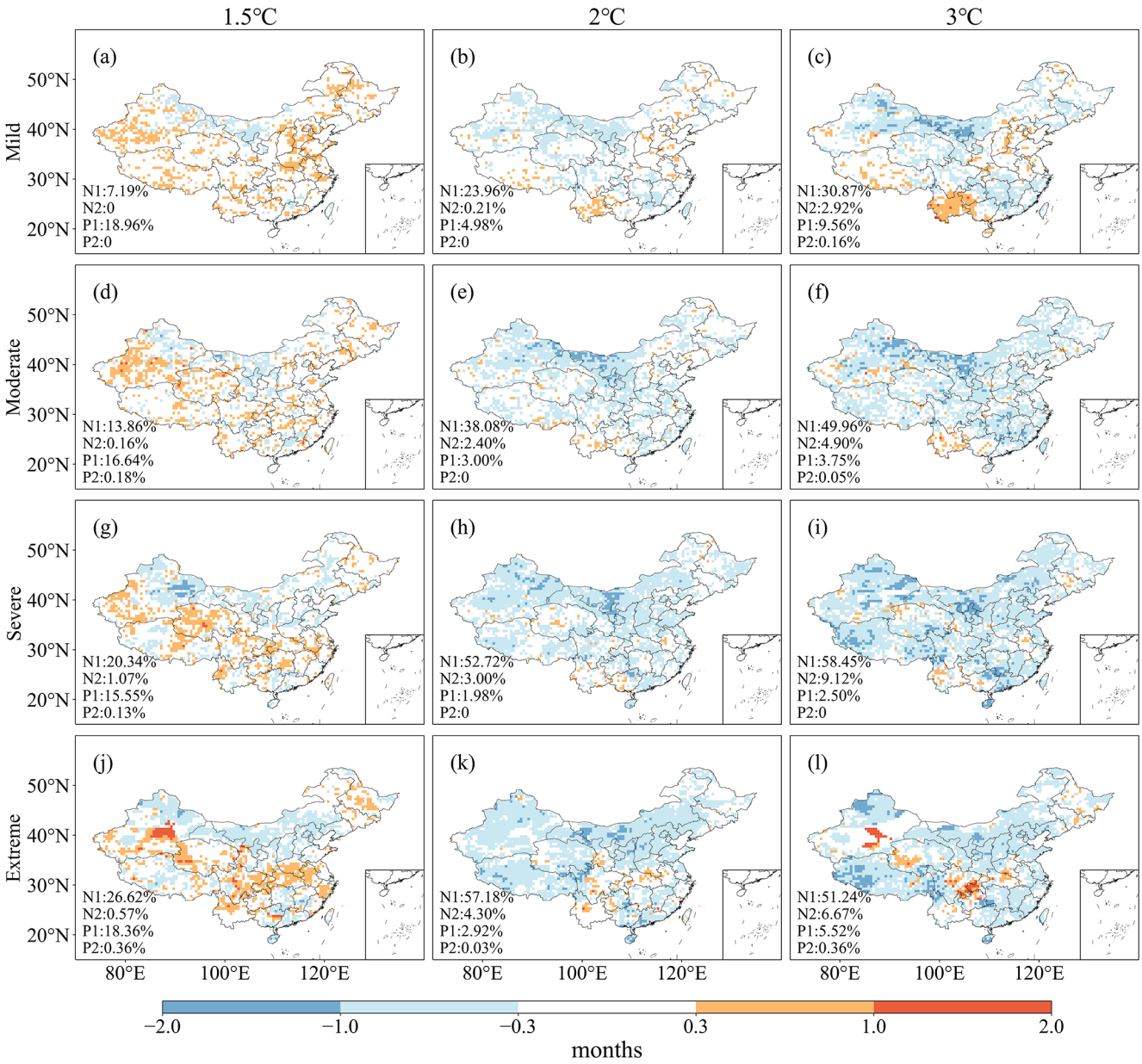

Fig. 10 Difference in occurrence month of the first (a–c) mild, (d–f) moderate, (g–i) severe, and (j–l) extreme CDH events under the three warming targets compared to 1981–2010. N denotes a negative value indicating an earlier occurrence of CDH events. N1 and N2 denote the percentage of grids with differences falling within the ranges of $[-1, -0.3)$ and $[-2, -1)$, respectively, relative to the total number of grids. P denotes a positive value indicating a later occurrence of CDH events. P1 and P2 denote the percentage of grids with differences falling within the ranges of (0.3, 1] and (1, 2], respectively, relative to the total number of grids

significant increase in extreme weather events, such as droughts, heatwaves, and CDH events (Zhang et al. 2022a; Min et al. 2023). These events often do not occur in isolation, primarily due to the influence of land-atmosphere coupling mechanisms. During the summer, elevated temperatures lead to increased potential evapotranspiration demands, subsequently reducing soil moisture (Tang et al. 2018). This moisture deficits hinder vegetation's ability to uptake water, resulting in low actual evapotranspiration rates (Wang et al. 2021) and a significant transfer of sensible heat flux to the atmosphere, thereby intensifying surface temperatures (Otkin et al. 2018; Zhang et al. 2019). Furthermore, reduced precipitation is closely associated with decreased soil moisture, contributing to temperature rises (Chen et al. 2019). The concurrent occurrence of precipitation shortages and elevated temperatures may precipitate CDH events. Currently, the substantial emission of greenhouse gases has significantly elevated global temperatures (IPCC 2021). In such warmer climates, land-atmosphere feedback mechanisms are likely to induce

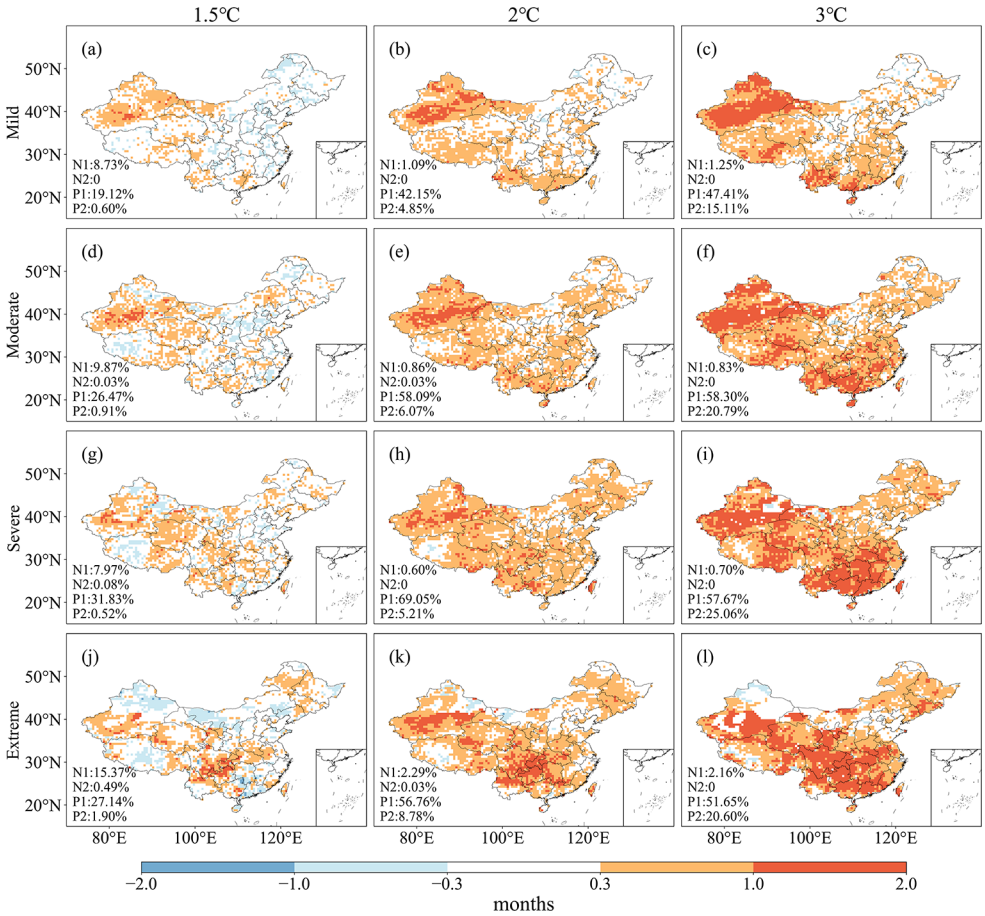

Fig. 11 Difference of occurrence month of the last (a–c) mild, (d–f) moderate, (g–i) severe, and (j–l) extreme CDH events per year under 1.5 °C, 2 °C, and 3 °C warming targets relative to reference period. N denotes a negative value indicating an earlier occurrence of CDH events. N1 and N2 denote the percentage of grids with differences falling within the ranges of [−1, −0.3) and [−2, −1), respectively, relative to the total number of grids. P denotes a positive value indicating a later occurrence of CDH events. P1 and P2 denote the percentage of grids with differences falling within the ranges of (0.3, 1] and (1, 2], respectively, relative to the total number of grids

more persistent, severe, and frequent CDH events, posing grave threats to ecological and environmental integrity (Bevacqua et al. 2022). Therefore, it is imperative to urgently quantify changes in CDH events across various warming scenarios.

Our findings indicate that CDH events are poised to become increasingly frequent in China with rising temperatures, aligning with the observations made by Zhang et al. (2023). This escalating frequency can be attributed to not just the land-atmosphere feedback mechanisms in a warming climate, but also to anomalies in atmospheric circulation (Wu et al. 2019b; Singh et al. 2022). For instance, the western Pacific subtropical high pressure has been identified as a crucial factor driving temperature increases (heatwaves) in EC (Liu and Zhou 2021). Similarly, the El Niño–Southern Oscillation (ENSO) plays a significant role in influencing the occurrence and variability of heatwaves and droughts (Lyon and Barnston 2005; Mukherjee et al. 2020). Furthermore, the strong negative-phase Arctic Oscillation and El Niño Modoki event are identified as primary contributors to drought in southwestern China (Yang et al. 2012).

Anthropogenic impacts on CDH events are also significant. Chen and Sun (2017) pointed out that the increases in CDH events in China is a consequence of the intricate interplay between natural and anthropogenic forcings. These anthropogenic forcings encompass greenhouse gas emissions, rapid urbanization, and land-use activities (Chen et al. 2019). In particular, substantial emissions of greenhouse gases have contributed to the ongoing elevation in average temperatures. This anthropogenic warming exacerbates the urban heat island effect and shapes the variability of CDH events. Hence, it is apparent that temperature rises stemming from human activities will increasingly influence CDH events (Chen and Sun 2017; Chen et al. 2019).

Currently, there is limited research on the occurrence times of CDH events, particularly in quantifying how these timings shift across various warming thresholds. With the increasing global temperatures, the onset of spring and summer seasons in China is advancing, while the onset of autumn and winter is being delayed (Chen et al. 2023b). This shift in the seasonal cycle, induced by global warming, is anticipated to impact the timing of CDH events within the country. Our findings reveal a tendency towards earlier occurrences of the first CDH event of the year and delayed occurrences of the last event. These findings align with Yang et al. (2021), who reported a trend towards earlier onset of extreme hot days across most of China. Additionally, Song et al. (2024) reported an increase in the frequency of spring

droughts in Southwest China, suggesting that the first CDH event of the year may also occur earlier due to intensified land-atmosphere feedback in warmer climates.

The earlier onset of the first CDH event and the later onset of the last CDH event extend the timeframe over which the CDH events occur each year. This elongation, coupled with elevated temperatures, is anticipated to significantly increase CDH events, thereby adversely impacting vegetation growth, food production, and human well-being (Haro-Monteagudo et al. 2019). Wei et al. (2023) pointed out that while the 2022 Indian spring heatwave initially enhanced urban vegetation greenness, the excessive temperatures during the heatwave period could compromise their vitality, thereby undermining their enduring benefits. Similarly, spring droughts can hinder crop sowing, complicating cultivation processes and leading to inadequate yields (Chen et al. 2023a). Winter droughts may induce xylem embolism in plants, causing dieback (Voltas et al. 2013). Consequently, the temporal shifts in CDH events undoubtedly portend more severe ramifications.

Predicting changes in CDH events under future warming scenarios involves inherent uncertainties and limitations. Firstly, considerable variation exists among CMIP6 model simulations due to differing internal variabilities and external forcings (Guo et al. 2021). Li et al. (2022) evaluated the accuracy of 41 historical and 3 integrated models in simulating global monthly precipitation, revealing substantial disparities in precision among different global climate models, especially across various geographical regions. Furthermore, they emphasized that MME can significantly enhance simulation capabilities. Consequently, our findings rely on the average outcomes from 12 CMIP6 model ensembles. Additionally, the choice of interpolation method introduces further uncertainty. This study employs bilinear interpolation for adjusting model resolutions to 0.5°×0.5°, a technique that smooths data fields and mitigates the occurrence of extremely high values, thereby resulting in lower data gradients (Chen and Knutson 2008; Li et al. 2022).

5 Conclusions

This study assessed the changes of CDH events across China under the three warming targets based on 12 model outputs from CMIP6. We focused on the spatio-temporal characteristics of CDH events with different magnitudes under 1.5 °C, 2 °C, and 3 °C warming targets. The findings may offer scientific insights for the formulation of effective policies to cope with the adverse consequences of CDH events. Our main conclusions are as follows:

(1) CDH events are projected to occur more frequently and with greater severity as warming levels increase, particularly under the SSP5-8.5 scenario. Specifically, the frequency of CDH events is anticipated to rise at rates of 0.035 events/decade, 0.109 events/decade, and 0.216 events/decade under SSP1-2.6, SSP2-4.5, and SSP5-8.5, respectively. The magnitude of CDH events is expected to increase more rapidly under SSP5-8.5 (0.04/decade) than the SSP2-4.5 (0.024/decade) and SSP1-2.6 (0.009/decade).

(2) At higher warming levels, the frequency and magnitude of CDH events are projected to increase significantly compared to historical periods. Specifically, if warming is limited to 1.5 °C, the frequency of CDH events would be reduced by 122.3% and 323.7% compared to scenarios of 2 °C and 3 °C warming, respectively. Regionally, NWC is expected to experience a greater increase in the frequency of mild CDH events, while SC is projected to see a higher frequency increase of moderate, severe, and extreme events. Overall, an increasing number of areas are expected to be impacted by CDH events, with the largest increase observed in the area affected by extreme events.

(3) As the warming level increases from 1.5 °C to 3 °C, the occurrence of the first CDH event per year becomes earlier, while the last CDH event occurs later. Notably, the proportion of regions where the first CDH event tends to occur earlier rises from 13.86% to 71.61%, whereas the number of regions experiencing a delayed last CDH event increases from 26.13% to 83.22%. This trend of earlier and later CDH event onset is initially observed in NWC and subsequently expands to EC. Furthermore, the magnitude of this advancement (delay) in the occurrence of the first (last) CDH event during the 3 °C warming period is more significant compared to the 1.5 °C and 2 °C periods, particularly in NWC.

Supplementary Information The online version contains supplementary material available at https://doi.org/10.1007/s00382-024-07215-0.

Author contributions Taizheng Liu, Yuqing Zhang, and Bin Guo contributed to the study conception and design. Data collection and analysis were performed by Taizheng Liu, Yuqing Zhang, and Yu Yin. Taizheng Liu prepared the first draft of the manuscript. Yuqing Zhang and Bin Guo reviewed and edited the manuscript. Jing Ge provided constructive comments on this study.

Funding This study is jointly supported by the National Natural Science Foundation of China (41807170, 41907384, and 42365010) and the Humanities and Social Science Fund of Ministry of Education of China (19YJCZH259).

Data availability The CMIP6 model data is obtained from https://esgf-node.llnl.gov/search/cmip6/. The CN05.1 gridded dataset can be downloaded after contacting Dr. Wang (wangjun@mail.iap.ac.cn).

Declarations

Conflict of interest The authors declare that they have no known competing financial interests or personal relationships that could have appeared to influence the work reported in this paper.

References

Adler RF, Gu G, Wang J-J, Huffman GJ, Curtis S, Bolvin D (2008) Relationships between global precipitation and surface temperature on interannual and longer timescales (1979–2006). J Geophys Research: Atmos 113:D22104

Bevacqua E, Zappa G, Lehner F, Zscheischler J (2022) Precipitation trends determine future occurrences of compound hot–dry events. Nat Clim Change 12:350–355

Byrne MP, O'Gorman PA (2018) Trends in continental temperature and humidity directly linked to ocean warming. Proceedings of the National Academy of Sciences 115:4863–4868

Chen C-T, Knutson T (2008) On the verification and comparison of extreme rainfall indices from climate models. J Clim 21:1605–1621

Chen H, Sun J (2017) Anthropogenic warming has caused hot droughts more frequently in China. J Hydrol 544:306–318

Chen L, Chen X, Cheng L, Zhou P, Liu Z (2019) Compound hot droughts over China: identification, risk patterns and variations. Atmos Res 227:210–219

Chen X, Li X, Jiang B, Su J, Zheng X, Wang G (2023a) Prediction of spring agricultural drought using machine learning algorithms in the southern Songnen Plain, China. Land Degrad Dev 34:3836–3849

Chen Y, Zhang Y, Li Y, Song S (2023b) Changes in lengths of the four seasons in China and the relationship with changing climate during 1961–2020. Int J Climatol 43:1349–1366

Forster PM, Maycock AC, McKenna CM, Smith CJ (2020) Latest climate models confirm need for urgent mitigation. Nat Clim Change 10:7–10

Guo H, Bao A, Chen T, Zheng G, Wang Y, Jiang L, De Maeyer P (2021) Assessment of CMIP6 in simulating precipitation over arid Central Asia. Atmos Res 252:105451

Hare B, Roming N, Schaeffer M, Schleussner C-F (2016) Implications of the 1.5°C limit in the Paris Agreement for climate policy and decarbonisation. Climate Analytics

Haro-Monteagudo D, Knox JW, Holman IP (2019) D-Risk: a decision-support webtool for improving drought risk management in irrigated agriculture. Comput Electron Agric 162:855–858

IPCC (2021) Summary for policymakers. In: Climate Change 2021: The Physical Science Basis. Contribution of Working Group I to the Sixth Assessment Report of the Intergovernmental Panel on Climate Change [Masson-Delmotte, V., P. Zhai, A. Pirani, S. L. Connors, C. Péan, S. Berger, N. Caud, Y. Chen, L. Goldfarb, M. I. Gomis, M. Huang, K, Leitzell, E. Lonnoy, J.B.R. Matthews, T. K. Maycock, T. Waterfield, O. Yelekci, R. Yu and B. Zhou (eds.)]. Cambridge, UK: Cambridge University Press

King AD, Karoly DJ, Henley BJ (2017) Australian climate extremes at 1.5°C and 2°C of global warming. Nat Clim Change 7:412–416

Kong Q, Guerreiro SB, Blenkinsop S, Li X-F, Fowler HJ (2020) Increases in summertime concurrent drought and heatwave in Eastern China. Weather Clim Extremes 28:100242

Li X, You Q, Ren G, Wang S, Zhang Y, Yang J, Zheng G (2019) Concurrent droughts and hot extremes in northwest China from 1961 to 2017. Int J Climatol 39:2186–2196

Li Z, Liu T, Huang Y, Peng J, Ling Y (2022) Evaluation of the CMIP6 precipitation simulations over global land. Earth's Future 10:e2021EF002500

Liu Z, Zhou W (2021) The 2019 autumn Hot Drought over the Middle-Lower reaches of the Yangtze River in China: early propagation, process evolution, and concurrence. J Geophys Research: Atmos 126:e2020JD033742

Luo M, Lau N-C, Liu Z, Wu S, Wang X (2022) An Observational Investigation of Spatiotemporally Contiguous heatwaves in China from a 3D perspective. Geophys Res Lett 49:e2022GL097714

Lyon B, Barnston AG (2005) ENSO and the spatial extent of Interannual Precipitation extremes in Tropical Land Areas. J Clim 18:5095–5109

Matthews TKR, Wilby RL, Murphy C (2017) Communicating the deadly consequences of global warming for human heat stress. Proceedings of the National Academy of Sciences 114:3861–3866

Meinshausen M, Nicholls ZRJ, Lewis J, Gidden MJ, Vogel E, Freund M, Beyerle U, Gessner C, Nauels A, Bauer N, Canadell JG, Daniel JS, John A, Krummel PB, Luderer G, Meinshausen N, Montzka SA, Rayner PJ, Reimann S, Smith SJ, van den Berg M, Velders GJM, Vollmer MK, Wang RHJ (2020) The shared socioeconomic pathway (SSP) greenhouse gas concentrations and their extensions to 2500. Geosci Model Dev 13:3571–3605

Min R, Gu X, Guan Y, Zhang X (2023) Increasing likelihood of global compound hot-dry extremes from temperature and runoff during the past 120 years. J Hydrol 621:129553

Mukherjee S, Ashfaq M, Mishra AK (2020) Compound drought and heatwaves at a global scale: the role of natural climate variability-associated synoptic patterns and land-surface energy budget anomalies. J Geophys Research: Atmos 125:e2019JD031943

Nam W-H, Hayes MJ, Svoboda MD, Tadesse T, Wilhite DA (2015) Drought hazard assessment in the context of climate change for South Korea. Agric Water Manage 160:106–117

Otkin JA, Svoboda M, Hunt ED, Ford TW, Anderson MC, Hain C, Basara JB (2018) Flash droughts: a review and assessment of the challenges imposed by rapid-onset droughts in the United States. Bull Am Meteorol Soc 99:911–919

Schleussner CF, Lissner TK, Fischer EM, Wohland J, Perrette M, Golly A, Rogelj J, Childers K, Schewe J, Frieler K, Mengel M, Hare W, Schaeffer M (2016) Differential climate impacts for policy-relevant limits to global warming: the case of 1.5°C and 2°C. Earth Syst Dynam 7:327–351

Singh J, Ashfaq M, Skinner CB, Anderson WB, Mishra V, Singh D (2022) Enhanced risk of concurrent regional droughts with increased ENSO variability and warming. Nat Clim Change 12:163–170

Song X, Chen H, Chen T, Huang Q, Deng S, Yang N (2024) Spatial and temporal variations of spring drought in Southwest China and its possible teleconnection with the global climate events. J Hydrology: Reg Stud 51:101655

Su B, Huang J, Fischer T, Wang Y, Kundzewicz ZW, Zhai J, Sun H, Wang A, Zeng X, Wang G, Tao H, Gemmer M, Li X, Jiang T (2018) Drought losses in China might double between the 1.5°C and 2.0°C warming. Proceedings of the National Academy of Sciences 115:10600–10605

Su B, Xiao C, Zhao H, Huang Y, Dou T, Wang X, Chen D (2022) Estimated changes in different forms of precipitation (snow, sleet, and rain) across China: 1961–2016. Atmos Res 270:106078

Sun Y, Zhang X, Zwiers FW, Song L, Wan H, Hu T, Yin H, Ren G (2014) Rapid increase in the risk of extreme summer heat in Eastern China. Nat Clim Change 4:1082–1085

Sun Y, Zhang X, Ren G, Zwiers FW, Hu T (2016) Contribution of urbanization to warming in China. Nat Clim Change 6:706–709

Tang G, Behrangi A, Ma Z, Long D, Hong Y (2018) Downscaling of ERA-Interim temperature in the Contiguous United States and its implications for rain–snow partitioning. J Hydrometeorol 19:1215–1233

UNFCCC (2015) Adoption of the Paris Agreement. In. FCCC/CP/2015/L. 9/Rev. 1

Vautard R, Gobiet A, Sobolowski S, Kjellström E, Stegehuis A, Watkiss P, Mendlik T, Landgren O, Nikulin G, Teichmann C, Jacob D (2014) The European climate under a 2°C global warming. Environ Res Lett 9:034006

Voltas J, Camarero JJ, Carulla D, Aguilera M, Ortiz A, Ferrio JP (2013) A retrospective, dual-isotope approach reveals individual predispositions to winter-drought induced tree dieback in the southernmost distribution limit of scots pine. Plant Cell Environ 36:1435–1448

Wang W, Zhang Y, Guo B, Ji M, Xu Y (2021) Compound droughts and heat waves over the Huai River Basin of China: from a perspective of the magnitude index. J Hydrometeorol 22:3107–3119

Wang L, Wang WJ, Du H, Shen X, Wu Z, Ma S, Liu Z, Jiang M (2022) Was warming amplified under drought conditions across China in observations and future projections? Earth's Future 10:e2021EF002614

Wei H, Chen B, Wu S, Xu B (2023) Impact of early heat anomalies on urban tree cooling efficiency: evidence from spring heatwave events in India. Int J Appl Earth Obs Geoinf 120:103334

Wu J, Gao X-J (2013) A gridded daily observation dataset over China region and comparison with the other datasets. Chin J Geophys 56:1102–1111

Wu X, Hao Z, Hao F, Singh VP, Zhang X (2019a) Dry-hot magnitude index: a joint indicator for compound event analysis. Environ Res Lett 14:064017

Wu X, Hao Z, Hao F, Zhang X (2019b) Variations of compound precipitation and temperature extremes in China during 1961–2014. Sci Total Environ 663:731–737

Wu H, Su X, Singh VP (2021) Blended dry and hot events index for monitoring dry-hot events over Global Land Areas. Geophys Res Lett 48:e2021GL096181

Yang J, Gong D, Wang W, Hu M, Mao R (2012) Extreme drought event of 2009/2010 over southwestern China. Meteorol Atmos Phys 115:173–184

Yang Y, Tang J, Wang S, Liu G (2018) Differential impacts of 1.5 and 2°C warming on Extreme events over China using statistically downscaled and Bias-corrected CESM low-warming experiment. Geophys Res Lett 45:9852–9860

Yang Y, Lin Z, Luo L, Zhang Y, Li Z (2021) Inhomogeneous trends in the onset date of extreme hot days in China over the last five decades. Atmospheric Ocean Sci Lett 14:100080

Yin Z, Zhou B, Duan M, Chen H, Wang H (2023) Climate extremes become increasingly fierce in China. Innov (Camb) 4:100406

Yu R, Zhai P (2020) More frequent and widespread persistent compound drought and heat event observed in China. Sci Rep 10:14576

Zampieri M, Ceglar A, Dentener F, Toreti A (2017) Wheat yield loss attributable to heat waves, drought and water excess at the global, national and subnational scales. Environ Res Lett 12:064008

Zhang Y, You Q, Mao G, Chen C, Ye Z (2019) Short-term concurrent drought and heatwave frequency with 1.5 and 2.0°C global warming in humid subtropical basins: a case study in the Gan River Basin, China. Clim Dyn 52:4621–4641

Zhang Y, Yang X, Chen C (2021) Substantial decrease in concurrent meteorological droughts and consecutive cold events in Huai River Basin, China. Int J Climatol 41:6065–6083

Zhang G, Wang H, Gan TY, Zhang S, Shi L, Zhao J, Su X, Song S (2022a) Climate change determines future population exposure to summertime compound dry and hot events. Earth's Future 10:e2022EF003015

Zhang Q, She D, Zhang L, Wang G, Chen J, Hao Z (2022b) High sensitivity of compound drought and heatwave events to global warming in the future. Earth's Future 10:e2022EF002833

Zhang X, Chen Y, Fang G, Xia Z, Yang Y, Duan W, Xia Q, Li S (2022c) Future changes in extreme precipitation from 1.0°C more warming in the Tienshan Mountains, Central Asia. J Hydrol 612:128269

Zhang Y, Hao Z, Zhang Y (2023) Agricultural risk assessment of compound dry and hot events in China. Agric Water Manage 277:108128

Zhuang Y, Zhang J, Liang J (2021) Projected temperature and precipitation changes over Major Land regions of the Belt and Road Initiative under the 1.5°C and 2°C climate targets by the CMIP6 Multi-model Ensemble. Clim Environ Res 26:374–390

Zscheischler J, Westra S, van den Hurk BJJM, Seneviratne SI, Ward PJ, Pitman A, AghaKouchak A, Bresch DN, Leonard M, Wahl T, Zhang X (2018) Future climate risk from compound events. Nat Clim Change 8:469–477